November 6, 2018
Preprint typeset using LaTeX style emulateapj v. 11/26/04

ANALYSIS AND MODELING OF COSMIC MICROWAVE BACKGROUND RADIATION BASED ON FOUR-YEAR COBE-DMR DATA

Jowita Borowska
Institute of Theoretical Astrophysics, University of Oslo, P.O. Box 1029 Blindern, N-0315 Oslo, Norway; jowitab@student.matnat.uio.no
Submitted November 6, 2018

ABSTRACT

Analysis of the four-year COBE-DMR data taken at frequencies 53 and 90 GHz has been performed. Our goal was to determine the maximum-likelihood values of parameters Q, corresponding to the amplitude of the CMB spectrum, and n, corresponding to its tilt. In order to do that, we have compared observational data with the class of theoretical models parametrized by Q and n. Various combinations of 60 different values in the range $Q \in [0, 50]$ and $n \in [-1, 3]$ yielded the best-fit estimates: $Q_{53\mathrm{GHz}} = 18.3 \pm 4.4\ \mu$K, $Q_{90\mathrm{GHz}} = 19.6 \pm 6.6\ \mu$K and $n_{53\mathrm{GHz}} = 0.93 \pm 0.32$, $n_{90\mathrm{GHz}} = 1.24 \pm 0.51$. Results are in agreement with the inflation theory, predicting a rapid expansion at the beginning of the Universe.

Subject headings: cosmic microwave background - cosmology: observations

1. INTRODUCTION

The cosmic microwave background (CMB) radiation consists of the photons released about 380 000 years after the Big Bang, thus it is considered to be a reflection of the early Universe. Before the CMB was released, temperature and density of the particles were extremely high and the interactions between them were very frequent. For this reason, photons were tightly coupled to the ordinary matter (such as electrons and protons) and could not propagate over longer distances - the Universe was opaque. Nevertheless, the Universe was expanding and simultaneously cooling. When it reached a temperature of about 3000 K, electrons combined with protons, forming neutral hydrogen atoms. Therefore, photons, now decoupled from electrons, were able to move unhindered through the transparent Universe (ESA). Further expansion has led to wavelength elongation of CMB photons (*redshift* to microwave-range of the electromagnetic spectrum), so that their effective temperature has decreased to approximately 2.725 K. This temperature value can be measured almost uniformly across the sky, with small fluctuations. The CMB anisotropy, caused by these very temperature variations, represents the density distribution of the early Universe - the hotter the photons, the higher the density was at the time they were released (Eriksen & Ruud 2016).

Standard Big Bang theory implies relatively gradual expansion throughout the whole history of the Universe. However, according to the inflation theory, during the first few moments of the Universe (10^{-32} seconds) it underwent a rapid exponential expansion that caused an increase of the Universe size by a factor of about 10^{30}. Therefore, random quantum fluctuations at the beginning of the Universe had been amplified to the cosmologically large scales during the inflation epoch (ESA).

Detection and precise measurment of the CMB intensity spectrum provide us with information about the Universe shortly after the Big Bang. In 1989, NASA launched Cosmic Background Explorer (COBE) in order to acquire necessary data. COBE carried three instruments - Far Infrared Absolute Spectrophotometer (FIRAS), to compare the CMB spectrum to the blackbody radiation; Diffuse Infrared Background Experiment (DIRBE), to search for the cosmic infrared background; as well as Differential Microwave Radiometer (DMR), to map the cosmic radiation with high accuracy (NASA 2008). In the following paper, analysis of the four-year data provided by the latter instrument - DMR - is performed. Comparison between the real CMB observations and mathematical predictions enables construction of the best model for the evolution of the Universe. We consider the observations from 53 GHz and 90 GHz frequency channels to find the best-fit estimates of the cosmological inflationary parameters, Q and n, occuring in the data model, described later in detail (where Q corresponds to the *amplitude* and n to the *tilt* of the CMB spectrum).

2. METHOD

Hereafter, the data model and description, as well as maximum likelihood analysis are developed following Eriksen & Ruud (2016).

2.1. *Mathematical model of data*

Observations of CMB can be approximated by the multi-variate centered Gaussian distribution (mean, $\mu = 0$),

$$p(\mathbf{x}) \propto \frac{1}{\sqrt{|\mathbf{C}|}} e^{-\frac{1}{2}\mathbf{x}^{\mathrm{T}}\mathbf{C}^{-1}\mathbf{x}}, \tag{1}$$

where data points are collected into vector $\mathbf{x}$ and $\mathbf{C} \equiv \langle \mathbf{x}\mathbf{x}^t \rangle$ is its covariance matrix. The diagonal entries of the covariance matrix are the variances of each one-dimensional variate from the data vector, σ_i^2, while the off-diagonal entries are covariances between j-th and i-th variate (measurment of how two elements vary together), σ_{ij}. In order to derive an expression for the covariance matrix, we introduce the following data model,

$$d(\hat{n}) = s(\hat{n}) + n(\hat{n}) + f(\hat{n}), \tag{2}$$

where d is the total signal observed in direction $\hat{n}$, s is purely CMB, n represents noise and f - foreground signals, obscuring the true cosmological signal (e.g. radiation from the Milky Way). Assuming no correlation

between these factors, the covariance matrix of the data model, d, is found to be

$$\begin{aligned}\mathbf{C} \equiv \langle \mathbf{d}\mathbf{d}^{\mathrm{T}} \rangle &= \langle (\mathbf{s}+\mathbf{n}+\mathbf{f})(\mathbf{s}+\mathbf{n}+\mathbf{f})^{\mathrm{T}} \rangle \\ &= \langle \mathbf{s}\mathbf{s}^{\mathrm{T}} \rangle + \langle \mathbf{n}\mathbf{n}^{\mathrm{T}} \rangle + \langle \mathbf{f}\mathbf{f}^{\mathrm{T}} \rangle \equiv \mathbf{S}+\mathbf{N}+\mathbf{F}.\end{aligned} \tag{3}$$

Here $\mathbf{S}$, $\mathbf{N}$ and $\mathbf{F}$ are covariance $N_{pix} \times N_{pix}$ matrices for each corresponding signal source alone (we have used the fact that all cross-products have zero mean due to no correlation).

Noise, $\mathbf{N}$: We assume the Gaussian distribution of the noise, with no correlation between i-th and j-th pixel, so that the resulting covariance matrix has the usual one-dimensional variance values as the entries along the diagonal and zeros elsewhere - diagonal matrix with elements:

$$N_{ij} = \langle n_i n_j \rangle = \sigma_i^2 \delta_{ij}. \tag{4}$$

CMB signal, $\mathbf{S}$: We model CMB field as Gaussian and isotropic but correlated between pixels. The resultant expression for the pixel-pixel covariance matrix is then

$$S_{ij} = \frac{1}{4\pi} \sum_{l=0} (2l+1)(b_l p_l)^2 C_l P_l(cos\theta_{ij}), \tag{5}$$

where l quantifies the effective wavelength, b_l is the instrumental beam and p_l is the pixel window (both given as the data sets and described more closely in the next section), $P_l(cos\theta_{ij})$ are the Legendre polynomials of the angle between pixels i and j, while C_l is the *power spectrum*. It is the power spectrum that ties observations together with the cosmological models of the evolution of the Universe. Estimating parameters occuring in the C_l-function to match the CMB data most accurately leads to finding the best model of the real Universe, as already mentioned. The class of models, we introduce for further use, is parametrized by an amplitude, Q, and a spectral index, n,

$$C_l = \frac{4\pi}{5} Q^2 \frac{\Gamma(l+\frac{n-1}{2})\Gamma(\frac{9-n}{2})}{\Gamma(l+\frac{5-n}{2})\Gamma(\frac{3+n}{2})}. \tag{6}$$

We set $C_0 = C_1 = 0$ (due to the removal of monopole, $l = 0$, and dipole, $l = 1$, described later more closely) and simplify the expression for $l = 2$ to $C_2 = 4\pi/5Q^2$. Moreover, because of the recursive property of the gamma function, $\Gamma(1+x) = x\Gamma(x)$, C_l corresponding to the successive l-values (and given by formula 6) can easily be evaluated using the previous one, C_{l-1}. The algorithm we follow is then

$$\begin{aligned} C_{l=0} &= 0, \\ C_{l=1} &= 0, \\ C_{l=2} &= \frac{4\pi}{5} Q^2, \\ C_{l=3,4,...} &= C_{l-1} \frac{l-1+\frac{n-1}{2}}{l-1+\frac{5-n}{2}}. \end{aligned} \tag{7}$$

Computations (with use of Python) are performed up to $l_{max} = 47$, for combinations of 60 different values of both Q and n parameters, varying in the range $Q \in [0, 50]$ and $n \in [-1, 3]$.

Foregrounds, $\mathbf{F}$: The COBE instrument providing the data for our analysis, DMR, measures just the difference between two points on the sky, not their absolute values (as the name *Differential Microwave Radiometer* would suggest). Therefore, information about the true monopole ($l = 0$) cannot be acquired from DMR measurments (although it was established by FIRAS instrument) and we have to exclude its possible effect from our map. Effect of the observed dipole ($l = 1$) also has to be removed, since it is impossible to distinguish between the true cosmological CMB dipole and the one being a result of the Doppler shifted (due to Earth's motion through the space) CMB monopole. Foreground covariance matrix ($\mathbf{F}$ in formula 3) is introduced to marginalize over any monopole and dipole components in the map and takes the form

$$\mathbf{F} = \lambda \mathbf{f}\mathbf{f}^{\mathrm{T}}, \tag{8}$$

where λ is some large constant (chosen to be 10^3) and $\mathbf{f}\mathbf{f}^{\mathrm{T}}$ is the outer product of a known structure or template on the sky, we marginalize over, with itself. To account for the monopole, λ is added to the total covariance matrix ($\mathbf{f}$ is then just a constant equal 1), and for the dipole - we use each of the unit direction vector components given in the data set, so that

$$\mathbf{F} = \lambda + \lambda(\mathbf{x}\mathbf{x}^{\mathrm{T}} + \mathbf{y}\mathbf{y}^{\mathrm{T}} + \mathbf{z}\mathbf{z}^{\mathrm{T}}). \tag{9}$$

2.2. *Likelihood analysis*

In order to determine which mathematical model fits observations most accurately, we are seeking best-fit values of the Q and n parameters occuring in the power spectrum expression (formula 6, 7). The method being followed is so-called *maximum-likelihood* framework. It is important to note the distinction between likelihood and probability - likelihood attaches to hypotheses, while probability attaches to possible results and must sum up to 1 (unlike likelihood), Gallistel (2015). The likelihood function quantifies the probabilty of obtaining a data set, given the mathematical model with specific parameters,

$$\mathcal{L}(Q, n) = p(\mathbf{d}|Q, n), \tag{10}$$

where $\mathbf{d}$ is the data vector. This function enables finding best-fit values of Q and n as the parameters giving the maximum likelihood (or being the weighted mean of one-dimensional distribution, as explained later). The joint disribution above is the multi-variate Gaussian given by equation 1, with $\mathbf{d}$ as its variable. Commonly, the logharitmic likelihood is introduced and considered instead of the likelihood itself, to prevent from numerical errors. The likelihood and log-likelihood then take the form

$$\mathcal{L}(Q, n) = p(\mathbf{d}) \propto \frac{1}{\sqrt{|\mathbf{C}|}} e^{-\frac{1}{2}\mathbf{d}^{\mathrm{T}}\mathbf{C}^{-1}\mathbf{d}} \tag{11}$$

$$\Rightarrow -2 \log \mathcal{L}(Q, n) = \log|\mathbf{C}| + \mathbf{d}^{\mathrm{T}}\mathbf{C}^{-1}\mathbf{d} + \text{constant}. \tag{12}$$

The latter is evaluated for various combinations of Q and n values, resulting in the two-dimensional contour plot of the likelihood.

To make computations faster, we use the Cholesky decomposition of the covariance matrix, $\mathbf{C} = \mathbf{L}\mathbf{L}^{\mathrm{T}}$, yielding the lower triangular matrix, $\mathbf{L}$. The determinant occuring in expression 11 is then

$$|\mathbf{C}| = \det\mathbf{L}\ \det(\mathbf{L})^{\mathrm{T}} = (\det\mathbf{L})^2 = (L_{11} \cdot L_{22} \cdot ...)^2$$
$$\Rightarrow \log|\mathbf{C}| = 2\log(L_{11} \cdot L_{22} \cdot ...) = 2\log L_{11} + 2\log L_{11} + ...$$

as the determinant of a triangular matrix is the product over all its diagonal elements, L_{ii} (computed up to $i =$

1941, the number of data points). Subsequently, we solve the equation

$$\mathbf{L}\mathbf{x} = \mathbf{d},$$

in order to rewrite $\mathbf{d}^{\mathrm{T}}\mathbf{C}^{-1}\mathbf{d}$ to much simpler $\mathbf{x}^{\mathrm{T}}\mathbf{x}$, where $\mathbf{x} = \mathbf{L}^{-1}\mathbf{d}$. Above components are then assembled to form the log-likelihood, $-2\log\mathcal{L}(Q,n)$.

Further, we find the one-dimensional marginal best-fit values for each parameter alone by integration,

$$\mathcal{L}(Q) = \int \mathcal{L}(Q,n)\mathrm{d}n, \tag{13}$$

$$\mathcal{L}(n) = \int \mathcal{L}(Q,n)\mathrm{d}Q. \tag{14}$$

Integration itself is performed using the composite Simpson's rule, and resultant likelihood as the function of each parameter individually is plotted. Then, we determine the best-fit values of Q and n as the weighted mean of the respective distributions (where weights correspond to the likelihood of each value) and their uncertainties as the weighted standard deviation. Mode of the distribution is also measured, as it represents the maximum likelihood value.

3. DATA

COBE-DMR instrument performed observations at three different frequencies: 31.5, 53 and 90 GHz. We choose to consider 53 and 90 GHz band, corresponding to the frequency channels burdened with the least foreground contamination and the lowest noise. On figure 1, CMB maps representing the data acquired at these frequencies are shown (following the dipole subtraction). It can be noticed that some regions of the sky are heavily dominated by foregrounds. This concerns mostly the Galactic plane, due to the significant radio emission from the Milky Way. We choose, therefore, to exclude the area around the Galactic plane from the data, using a mask - see figure 2. Here, the Galactic emission model (subtracted from the original 53 GHz map) is based on far-infrared and radio continuum observations. Thus, we account for the foreground signals from monopole and dipole by introducing the foreground covariance matrix (expression 9), $\mathbf{F}$, while the pixels strongly contaminated due to Milky Way radiation are simply removed from the analyzed data set.

In order to estimate CMB fluctuations from the real data, it is crucial to distinguish between the instrumental noise and the true cosmological noise, being CMB itself. On this account, we are given the list of standard deviations of the instrumental noise associated with each pixel, σ_p. The variances, σ_p^2, are diagonal entries of the introduced noise covariance matrix (expression 4), $\mathbf{N}$, where

$$\sigma_p = \frac{\sigma_0}{\sqrt{N_{obs,p}}}.$$

Here σ_0 is noise per measurment and $N_{obs,p}$ is the number of measurments made for a pixel p. During the entire 4-year period, the COBE satellite rotated and precessed in near-polar orbit, following the day-night terminator. As a result, the DMR performed observations of the entire sky over a six-month period (NASA 2008). COBE's effective scanning strategy has an impact on the noise (uncertainties) associated with

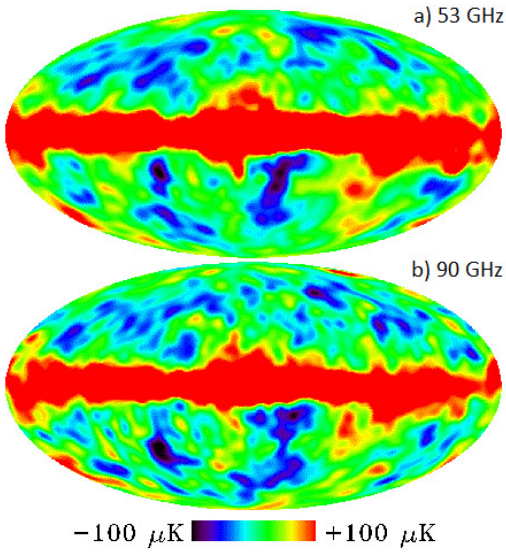

FIG. 1.— Maps (Mollweide projection) based on observations made by COBE-DMR during the entire 4-year mission at a) 53 GHz and b) 90 GHz. Both maps have been smoothed to an effective angular resolution of 10 degrees and the dipole component has been subtracted. Source: NASA

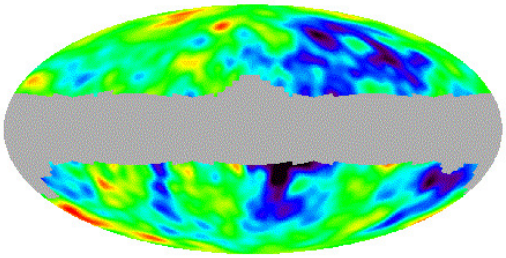

FIG. 2.— Reduced 53 GHz map - following both the dipole and model of the Galactic emission subtraction. Pixels excluded from the analysis are marked in grey (mask). Source: NASA

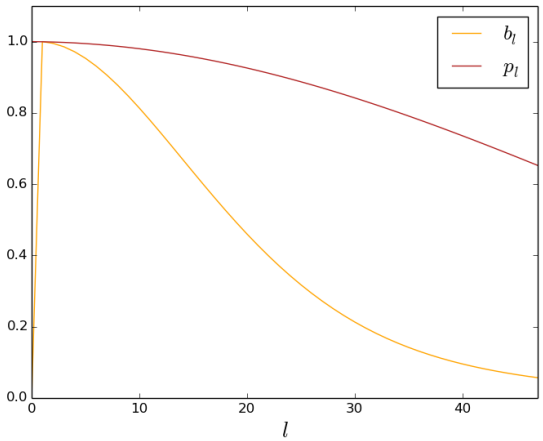

FIG. 3.— Plotted data points of the instrumental beam, b_l, and pixel window, p_l, with l (quantifying the wavelength of a given mode) varying up to $l_{max} = 47$.

each measured pixel. For instance, the Ecliptic plane is burdened with the biggest noise, since the satellite was designed to spend less time making measurments in this region, in order to avoid looking at the Sun. The more time COBE spent on the observations in a given region, the lower the noise.

Furthermore, we account for the instrumental beam (*point spread function*), b_l, which is the function defining how large area of the sky is seen by the instrument at any given time. The Legendre transform of the real-space beam function is tabulated in the file we use for analysis, which clearly decreases with increasing l when plotted (see figure 3). Since bigger l corresponds to the shorter wavelength of the mode (in the spherical harmonic decomposition), high l corresponds to smaller physical scales, while low l - to larger areas. The beam of COBE-DMR extends 7 degrees, smoothing the maps shown on figure 1, and giving an effective angular resolution of 10 degrees (NASA 2008).

Pixel window, p_l, that is occuring in the expression for CMB signal covariance matrix (eq. 5), $\mathbf{S}$, is also tabulated in the separate data file. Pixel window quantifies the effect of finite pixelization in the maps (prohibiting from detection of CMB variations smaller than the pixel-size). It behaves similarly to the beam, as can be seen on figure 3.

The set of data to be analyzed contains then: two files (for 53 and 90 GHz) with CMB measurments, consisting of 1941 unmasked pixels (size of each pix. corresponds to approximately 3.7° degrees) with associated unit direction vector components (x, y, z) and noise standard deviation, σ_p; COBE-DMR beam function, b_l, varying with l-values (up to $l = 64$); Pixel window function, p_l, with HEALPix (Hierarchical Equal Area isoLatitude Pixelization) of a sphere at $N_{\rm side} = 16$ (given also up to $l = 64$).

4. RESULTS

The whole mathematical model, closely described in the method section, has been implemented into the Python code. Analyzing given data set in the program and comparing it with the model parametrized by various combinations of Q and n parameters (60 different values varying in the range $Q \in [0, 50]$ and $n \in [-1, 3]$), results in the two-dimensional contour plots of the logharitmic likelihood, shown on figure 4. The Gaussian confidence regions 1σ (68%), 2σ (95%) and 3σ (99.7%) correspond to increase of $-2 \log \mathcal{L}(Q, n)$ from its minimum value by consequtively 2.3, 6.17 and 11.8 factor, which is marked by contour lines, together with the peak representation.

Further, we perform marginalization to remove one variable from the common likelihood distribution, by integrating over it (with use of the composite Simpson's rule). Resultant likelihood as the function of each parameter individually is shown on figure 5 (where the distribution is relative to the maximum likelihood value set to be equal 1). The one-dimensional marginal best-fit values are computed based on these distributions, and listed in table 1.

Due to the quite efficient implementation of the alghoritms, the runtime of the program determining log-likelihood has been about 41 minutes (for each frequency channel).

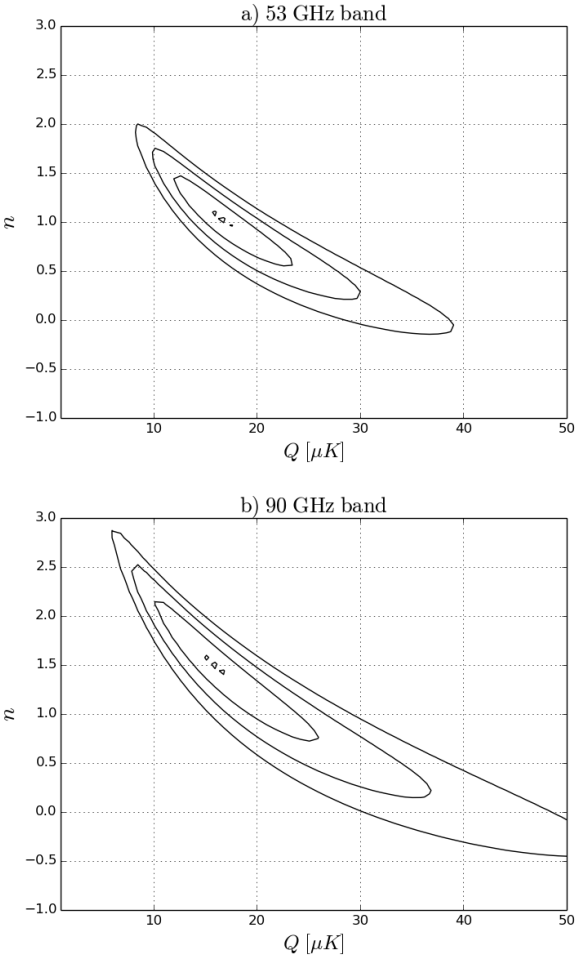

FIG. 4.— 2D-contour plots representing the likelihood for various combinations of (Q, n) in the model, compared with data at a) 53 GHz frequency channel and b) 90 GHz frequency channel. Likelihood peaks are marked by contour lines, together with the Gaussian confidence regions 68%, 95%, 99.7%.

TABLE 1
BEST-FIT VALUES OF PARAMETERS Q AND n DERIVED FROM MARGINAL DISTRIBUTION

Parameter		Frequency channel 53 GHz	90 GHz
Q (μK)	mode	16.8	15.9
	$\mu \pm \sigma$	18.3 ± 4.4	19.6 ± 6.6
n	mode	0.97	1.31
	$\mu \pm \sigma$	0.93 ± 0.32	1.24 ± 0.51

NOTE. — Mode corresponds to maximum likelihood value, while $\mu \pm \sigma$ is the weighted mean value ± standard deviation.

5. DISCUSSION AND CONCLUSION

One of the biggest achievements of the COBE satellite was measuring the intensity of CMB radiation, that followed a nearly perfect blackbody spectrum. The specific character of a blackbody spectrum is that the radiance temperature of a blackbody is the same at all frequencies (Wright 2009). This implies that the estimated Q and n parameters should be similar for both analyzed frequency channels, that is clearly in agreement with the estimatated values listed in table 1.

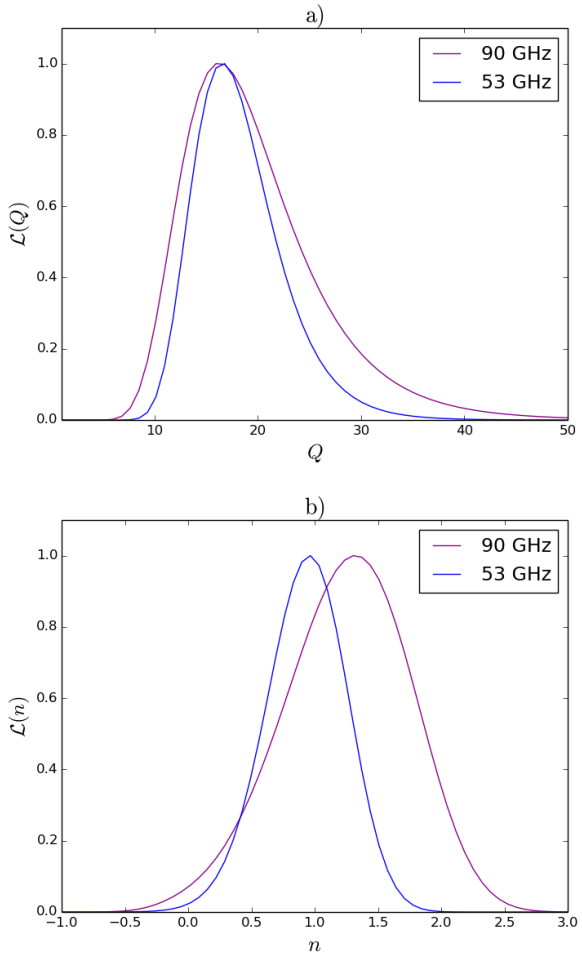

FIG. 5.— Likelihood distributions for each parameter individually: a) $\mathcal{L}(Q)$, b) $\mathcal{L}(n)$, plotted for both analyzed frequency channels (relative to the normalized maximal likelihood value).

The first detection of small spatial anisotriopies in the CMB temperature is also credited to the COBE-mission. They arose either during the inflation epoch or due to some topological defects in the early Universe. Commonly, it is assumed that these mechanisms produced a power-law on the form $P(k) \propto k^n$ (Pe'er 2017), where n is a spectral index that has been used for parametrization of our power spectrum model, C_l. The inflationary theory predicts that $n \approx 1$, which, again, is consistent with our estimates.

Fluctuations of the CMB temperature are very faint comparing to the almost uniform, on average 2.725 K, radiation field. Q parameter corresponds to the amplitude of these variations, so its maximum-likelihood estimate yields that the order of relative CMB fluctuations is about $16\mu K/2.7K \approx 6 \cdot 10^{-6}$. Because the distance between the opposite directions of the sky is so large, assuming standard Big Bang theory expansion, they could never have been in a causal contact with each other (the time light would travel between them exceeds the age of the Universe). Nevertheless, almost uniformity of CMB temperature, indicates that these regions must had been in contact in the past, which can be explained by the rapid initial expansion predicted by the inflation theory (NASA 2010).

Górski et al. (1994) get similar results for Q and n parameters. Small differences occur, for instance due to the fact that Górski analyzes two-year COBE-DMR data, while we have used the more accurate measurments - from the entire four-year mission. However, in both cases, the marginal likelihood distribution gives lower best-fit n-values than the two-dimensional joint distribution (that can be seen by comparing the position of peaks on 2D-contour plot from figure 4 with marginal estimates from table 1).

REFERENCES

Eriksen, H. K. and Ruud, T. M. (2016). Project assignment AST2210 - Analysis of four-year COBE-DMR data. Retrieved from: *http* : *//folk.uio.no/hke/AST*2210/*project_AST*2210*_cobe.pdf*

European Space Agency. (2000-2018). History of cosmic structure formation and The cosmic microwave background and inflation. Retrieved from: *www.esa.int/Our_Activities/Space_Science/*

Gallistel, C.R. (2015). Bayes for Beginners: Probability and Likelihood. Retrieved from: *www.psychologicalscience.org /observer/bayes−for−beginners−probability−and−likelihood*

Górski, K. M., Hinshaw, G., Banday, A. J., Bennett, C. L., Wright, E. L., Kogut, A. (1994). On determining the spectrum of primordial inhomogeneity from the COBE DMR sky maps: Results of two-year data analysis. *The Astrophysical Journal*, vol. 430, no. 2, pt. 2, p. L89-L92

NASA. (2008). LAMBDA - Data Products: COBE. Retrieved from: *https* : *//lambda.gsfc.nasa.gov/product/cobe/*

NASA. (2010). What is the Inlation Theory? Retrieved from: *https* : *//wmap.gsfc.nasa.gov/universe/bb_cosmo_infl.html*

Pe'er, A. (2017). Cosmic Microwave Background Anisotropy. Retrieved from: *http* : *//www.physics.ucc.ie /apeer/PY*4111/*CMB.pdf*

Wright, E. L. (2009). Cosmic Microwave Background. Retrieved from: *http* : *//www.astro.ucla.edu/ wright/CMB.html*